applied sciences

MDPI

Article

Effects of Aft-Body Extension Design on the Fundamental Characteristics of HWB Civil Aircraft

Yucheng Wang *, Gang Liu * and Guanxin Hong

School of Aeronautic Science and Engineering, Beihang University, Beijing 100191, China
* Correspondence: by1805145@buaa.edu.cn (Y.W.); lg@buaa.edu.cn (G.L.)

Abstract: The extension of aft-body fuselage has become an important trend in the design of Hybrid Wing Body (HWB) civil aircraft due to its improved effect on flight control authority of aircraft. However, it is still unclear how efficient the extension of aft-body will be in improving flight control authority and how it affects other aspects of the flight performance of HWB. To address these problems, this paper evaluated and compared the flight performances of four HWB configurations with different aft-body lengths. A physics-based Multidiscipline Design Optimization (MDO) platform was firstly constructed, and four optimal design works were developed based on this platform, with different static margin constraints. The configurations to be studied came from the results of the four optimization design works, which presented different aft-body lengths under the influence of correspondence between static stability margins and aft-body layout. By investigating these four HWB configurations with the weight, basic takeoff and landing performance, and flight control authority, we can determine the influence of the aft-body extension design on the performances of the HWB civil aircraft and provide advice for the layout design of the HWB aircraft.

Keywords: HWB civil aircraft; Multidiscipline Design Optimization; planform design; aft-body extension

check for updates

Citation: Wang, Y.; Liu, G.; Hong, G. Effects of Aft-Body Extension Design on the Fundamental Characteristics of HWB Civil Aircraft. *Appl. Sci.* **2022**, *12*, 8681. https://doi.org/10.3390/app12178681

Academic Editor: Jérôme Morio

Received: 14 July 2022
Accepted: 25 August 2022
Published: 30 August 2022

Publisher's Note: MDPI stays neutral with regard to jurisdictional claims in published maps and institutional affiliations.

Copyright: © 2022 by the authors. Licensee MDPI, Basel, Switzerland. This article is an open access article distributed under the terms and conditions of the Creative Commons Attribution (CC BY) license (https://creativecommons.org/licenses/by/4.0/).

1. Introduction

With the growing market requirements for fuel economy, noise, and emissions of civil aircraft, the research of novel configurations for civil aviation, such as Blended Wing Body [1–7], Double Bubble, Truss Braced Wing, Hybrid Wing body [8], Box Wing [9,10], etc., have become the focus of the industry. Among them, the HWB is an aircraft concept that adopts the integration of the fuselage and wing [11–14]. This configuration can reduce the wet area of the aircraft, thereby reducing the aircraft drag and improving the operation economy. At present, the extension of aft-body is one of the main design trends of HWB concept [15,16], which is mainly to increase the control arm of HWB to improve its takeoff and landing performance and flight control authority.

However, the current research on this design trend has the following two problems: First, although it is now accepted that the aft-body extension is designed to improve the short fuselage HWB aircraft with control arms to promote its takeoff and landing performance and control authority. The effect of aft-body extensions on these two aspects of performance is rarely mentioned in today's research, and there is uncertainty about the effect of aft-body extension on other basic flight-performance aspects, such as weight, while improving takeoff and landing and control authority. Moreover, there is a lack of planform design methods to obtain HWB civil configurations with different aft-body lengths. Therefore, this study developed a method to obtain an aft-body extension design from the perspective of planform optimization, and based on this method, this paper discusses the effects of aft-body extension on the HWB performance mentioned above, including weight, basic takeoff and landing performance, and flight control authority. Because of the high coupling between aerodynamic, weight, and stability-balance characteristics in the

concept design of HWB, which come from its highly integration of lifting fuselage, wings, and control surfaces, this paper needs to establish an MDO design platform for the HWB and study the characteristics mentioned above based on this platform.

The MDO method has long been used in the design of new-concept civil aircraft. Boeing used the WingMDO tool for early BWB multidisciplinary optimization, which uses the traditional vortex lattice method for aerodynamic estimation and the single-beam simplification assumption for structural weight estimation. Through a multidisciplinary optimization approach, adjusting the planform, center body airfoil shape, and torsional distribution, Boeing optimized the design of the BWB450 to achieve a statically stable trim (static stability margin = 5%) [17]. Lyu et al. established a high-fidelity multidisciplinary optimization platform based on the CFD (Computational Fluid Dynamics) method. Optimization constraints involve lift, trim, static stability margin, and the allowable bending moment of the central fuselage. In the aerodynamic module of MDO, a high-order model based on the Navier–Stokes equation is used. Due to the high-order aerodynamic calculation method, the shape of the aircraft does not change drastically during the optimization process, as the plane shape of the aircraft is not involved; only the spanwise torsion distribution of the wing is changed [18]. Thomas comprehensively studied the influence of various stability constraints on a 100-seat BWB layout design. In this author's research, a multi-objective optimization design framework was adopted. The optimization objective is not limited to cruise aerodynamic drag; it also combines the maximum/minimum takeoff weight [19]. MingHui Zhang et al. discussed the impact of two key constraints —static stability margin and thrust-specific fuel consumption (TSFC)—on the HWB optimization results [20].

According to previous studies on MDO aircraft, there are two conclusions. First, the multidisciplinary optimization design for an aircraft with blended wing and body can be divided into two types: planform change or not. The former includes the change of aircraft planform, and accordingly, its design space consists of parameters such as wing swept-back angle, wingspan, fuselage length and width, transition part width, etc., which can be used to realize the exploration of various potential configurations in the aircraft conceptual design stage. Due to the drastic changes in the aerodynamic shape, the kind of optimization is more suitable for using low-order aerodynamic models. The latter optimizes the layout of aircraft through parameters such as wing torsion distribution, cross-sectional airfoil, etc., under a fixed planform. Therefore, this kind of optimization is essentially a way of fine-tuning the aerodynamic shape based on a relatively fixed layout, and, thus, a high-order aerodynamic models can be used. Secondly, the static stability margin is a very important constraint in the MDO of HWB or BWB. Compared to the conventional TAW aircraft, the static stability margin has more influence on the resultant layout of HWB or BWB aircraft in the optimization due to the highly integrated wing-body.

In this paper, since the influence of the aft-body extension design on the main characteristics of the aircraft needs to be studied, a multidisciplinary optimization design with planform variation should be chosen, and the design space should include kinds of planform parameters. As for the optimization constraint, this paper adopts the longitudinal static stability margin as the main constraint for the following reason: there is a clear correspondence between the static stability margin and the planform of the aircraft, and the configurations with different planform (including different aft-body lengths) can be obtained by setting different static stability margin constraints in the optimization design.

Based on the above two premises, a physics-based MDO design planform was developed to obtain a family of configurations with different aft-body lengths of HWB by setting different static stability margins. Then, by evaluating, comparing, and analyzing the weight, basic takeoff, and landing performance, as well as flight control authority, of the aircrafts in the configuration family, we can obtain the influence of the aft-body extension design on the performance of the HWB civil aircraft, which provides advice for the layout design of the HWB civil aircraft.

2. MDO Optimization Platform

The optimization planform in this paper uses NSGAII (Nondominated Sorting Genetic Algorithm II) as the optimization algorithm, and the initial population is set to 120. NSGAII is a multi-objective optimization algorithm, and the optimization objectives in this paper are to maximize the cruise lift-to-drag ratio and minimize the maximum takeoff weight (MTOW). The whole optimization architecture is shown in Figure 1 and contains five modules with three constraints. The five modules are described in detail in later sections, and here we introduce the three levels of optimization constraints: (1) The cabin area, with reference to the cabin density of conventional TAW civil aircraft [21], should have a lower limit set to 300 m^2 for a 400-seat HWB civil aircraft. (2) There should be a clean configuration at cruise altitude and Mach number, meaning that the total aircraft pitch moment should be kept to zero when each control surface is in neutral position during cruise flight. (3) The stability and control constraint should be applied, which contains two aspects: One is the static stability margin constraint, which will largely determine the planform of the HWB, so by controlling the range of values of this constraint, different layouts of HWB configurations will be obtained. The other one is the basic control constraint, which is used to ensure that the resulting configuration is basically maneuverable. This constraint is determined by short-period frequency, ω_{nsp}, and the control anticipant parameter, $\frac{\Delta n}{\Delta \alpha}$, of the cruise state. The design has an acceptable maneuvering performance or not depending on whether the point $\left(\omega_{nsp}, \frac{\Delta n}{\Delta \alpha}\right)$ lies within the envelope of Class 2 flight quality.

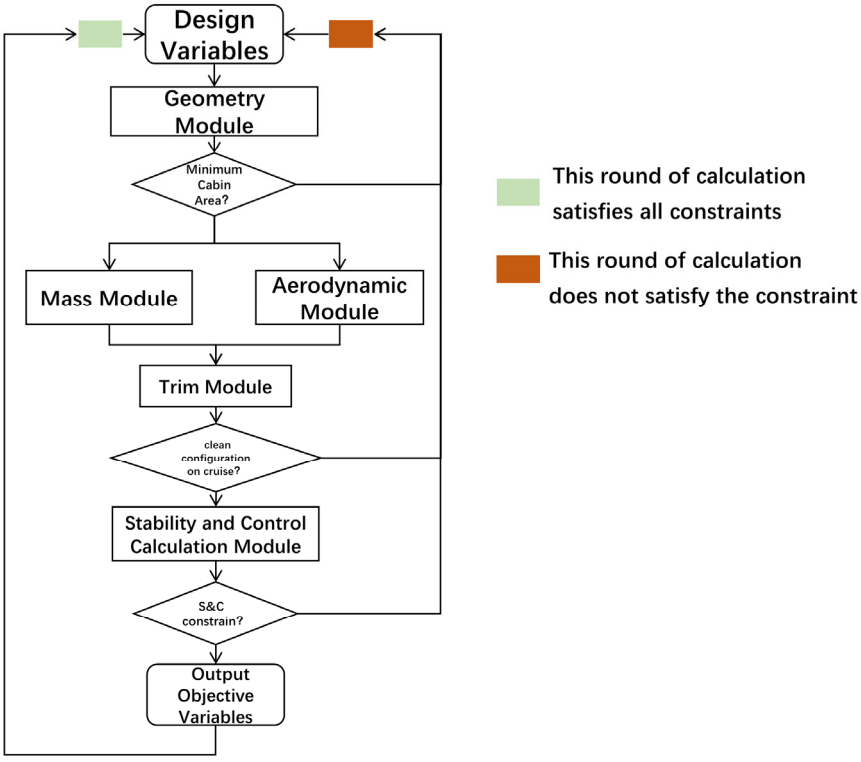


Figure 1. Program structure of the MDO design platform.

In this paper, the inputs to the MDO design platform are nine aircraft planform geometry parameters that can determine the main features of the aircraft's plan layout, and the lift-to-drag ratio, MTOW, and static stability margin of the design were set as output parameters. The entire MDO design program consists of five modules: geometry module, weight module, aerodynamic module, trim module, and stability and control characteristics calculation module. According to the Figure 1, the data flow unidirectionally in the above five calculation programs; that is, only the result of the planform planning of the HWB will determine the inertial characteristics of the aircraft, while the planform

and inertial characteristics will jointly determine the aerodynamic characteristics and S&C characteristics of the aircraft.

2.1. Geometry Module

As mentioned above, the input of the geometry module is also the input to the entire MDO design program, which is composed of 9 geometric parameters that determine the HWB planform; these 9 geometric parameters are shown in Figure 2. The functionalities of the geometry module include settling down the HWB baseline of planform; spline interpolation of the baseline of the planform to make its profile smooth for subsequent aerodynamic calculations; planning the cabin area and calculating the cabin area; and planning the main structure dimensions to provide geometric parameters for subsequent mass calculations.

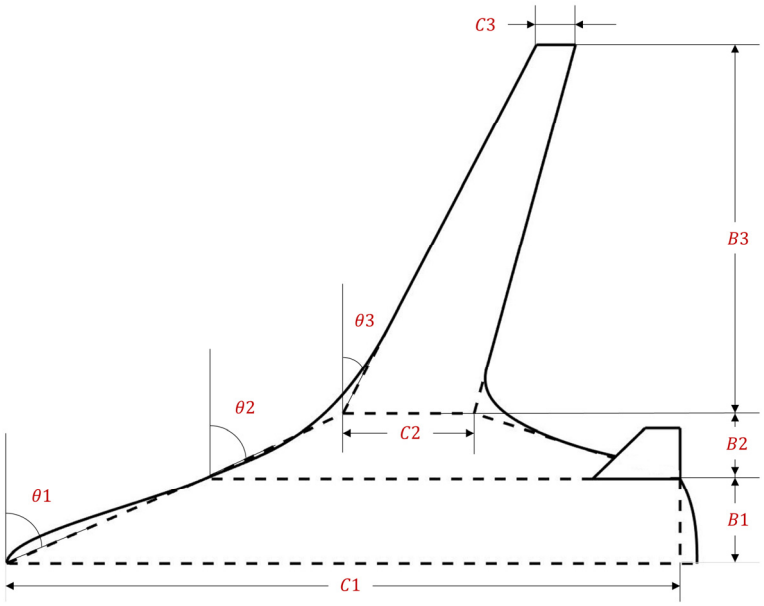


Figure 2. The planform parameters of HWB aircraft.

The 9 parameters of the geometry module together determine the planform of HWB aircraft, which consists of the center fuselage, the transition part, and the outer-wing section. In the specific calculation procedure, these 9 parameters are substituted into the geometric formulas to obtain the coordinates of eight points located in the aircraft construction coordinate system. These points are connected by straight lines to form the baseline of the planform (shown as black dashed lines in Figure 2). After the baseline is determined, the leading and trailing edges of the transition part and the leading edge of the center fuselage in the baseline are interpolated by cubic spline interpolation, and the resulting smooth profile (as shown by the solid black line in Figure 2) can be used in the subsequent trim and aerodynamic calculation modules.

The geometry module not only determines the planform of the aircraft but also divides the internal area of the aircraft for subsequent structural estimation. In the geometry module, the planform of the aircraft is divided into three parts: the yellow area is the passenger cabin area; the red area is the aft-body area, which is mainly used for the structural bearing of the engine weight; and the green area is the simplified shape of the outer-wing section (as shown in Figure 3).

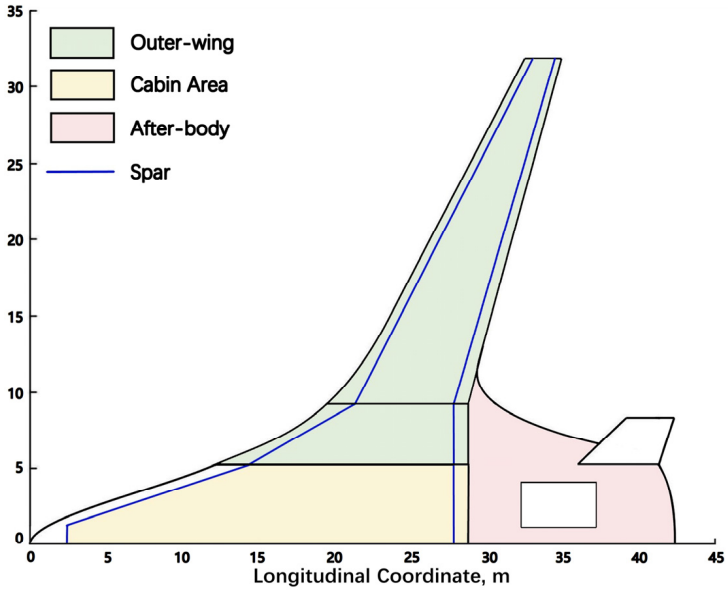


Figure 3. Internal layout of the HWB aircraft.

2.2. Weight Module

The weight module is a key part of the multidisciplinary optimization design, which will be used to estimate the mass of the configuration and its distribution and, thus, determine important parameters such as center of mass and moment of inertia, the results of which will also affect the static stability margin. The total mass of the aircraft includes the mass of several major components, including the structural mass, propulsion system, fixed airborne equipment, landing gear, fuel, crew, and cargo. The location of the center of mass of the entire aircraft is derived by combining the masses of the above major components and their locations.

The total mass of the aircraft is calculated by the following regression equation:

$$M_t = M_{cabin} + M_{aft} + D_o + M_V + Mr + M_{equi} + M_{prop} + M_{lg} + M_{load} + M_{cargo}, \quad (1)$$

The first five items on the right hand of the above equation are the structural masses of the whole aircraft, specifically the mass of the cabin part of the center body, the mass of the aft-body of the central fuselage, the mass of covers and webs, and the mass of ribs of the outer wing, which will change with the different parameters of the planform; the subsequent items are the items corresponding to the propulsion system, fixed airborne equipment, landing gear, fuel, crew, and cargo, which are set as constant values in the calculation. However, the positions of these parts have an influence on the calculation of the rotational inertia and the position of the center of mass of the entire aircraft.

The structural mass corresponding to the central body is divided into two parts, namely the cabin part and rear part, for which the mass calculation method of these two parts is given in the literature [22].

The two terms corresponding to the structural mass of the outer wing and transition part can be estimated by a method based on empirical equations, which is similar to the estimation methods of traditional wing [23]. Moreover, the masses of covers and webs in outer wing and transition part are as follows:

$$D_o = 0.85[\overline{N}M_T b^3 r_o e_o \sec\varphi_o \sec\gamma_o y_k^4 (1 + 0.375 y_k)]^{1/2} \times \left(\frac{S_o'}{S_o}\right)\left(\frac{\rho_o \overline{f}}{\overline{A}}\right)\left(\frac{c_k}{\tau_k}\right)_o^{0.25} \times 10^{-5}\text{kg}, \quad (2)$$

Furthermore, $\overline{f_a}$ is the ratio of allowable stress in the kink station between the transition part and center body to the allowable stress of the structural material:

$$\overline{f_a} = \frac{(f_a)_k}{(f_a)_{limit}}, \tag{3}$$

$$(f_a)_k = \overline{A}[0.727\overline{N}M_T A_o r_o (1+\lambda_o)\mathrm{s}\varphi_o \mathrm{s}\gamma_o y_k^2 \times \frac{(1+0.375y_k)}{e_o(c_k\tau_k)_o^{1.5}}]^{1/2}, \tag{4}$$

The mass of the rib structure in the outer wing and transition part is calculated as follows:

$$M_r = 4.4 S_o e_o (c_k\tau_k)_o^{1/2}(1+0.35\lambda_o)\rho_o \ \times 10^{-3}\mathrm{kg}, \tag{5}$$

As for the mass of the V-tail, the calculation can refer to the following equation:

$$M_V = 0.1 V_D S_V^{1.15}\mathrm{kg} \tag{6}$$

where V_D is the aircraft design speed and S_V is the wing area of the V-tail.

The coordinates of the center of mass of each major mass part are varied with the value of the planform geometric parameters, and the distribution of the main mass part is shown in the Figure 4. Based on the mass of each main part and its position, the total mass and moment of inertia, as well as the position of the center of mass of the entire aircraft, can be derived.

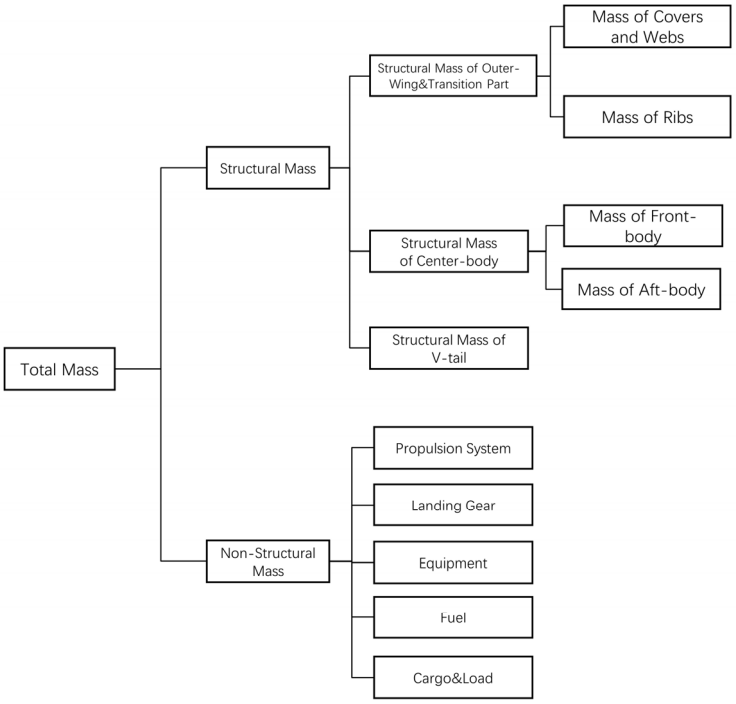


Figure 4. Structure of the weight module.

2.3. Aerodynamic Module

The main function of the aerodynamic module is to construct the aerodynamic model of the studied configuration, and the built aerodynamic model is then used for the aerodynamic calculation in the trim module and stability and control module. The optimization calculation in this paper has the following characteristics: first, the aircraft planform changes very drastically for the need of exploring different planform layout aircraft; second, the optimization process requires aerodynamic calculations for many cases. Based on the above two characteristics, this paper adopts the low-order method based on the potential flow theory, i.e., the vortex lattice method, for aerodynamic calculations. AVL (Athena Vortex Lattice), a general software for aerodynamic analysis based on the vortex lattice method, is used, which can realize fast and automatic calculation of aerodynamic characteristics of aircraft of different configurations in the form of batch files. Since the AVL calculation of aerodynamics requires the meshing of the aircraft geometry, it needs the whole aircraft's

shape information, which can be provided by the geometry module. Due to the limitation of theoretical assumptions, the vortex lattice method is only available for the calculation of lift and lift-induced drag, but not the calculation of friction drag and form drag. Therefore, this paper needs to introduce the FRICTION code based on the classical flat plate theory as a supplement to the vortex-lattice-method aerodynamic calculation software to realize the calculation of friction drag and form drag. This part of the calculation does not require the aircraft planform information; it requires only the average aerodynamic chord length and the airfoil parameters of three segments of the HWB, as well as the reference area of entire aircraft.

As mentioned before, the AVL calculation requires aircraft-shape information, which consists of two parts. The first part is the planform-shape information, which can be concretely reflected in the mesh model of AVL software, as shown in Figure 5. The planform shape is determined by the coordinates of the leading and trailing edges of several chordal sections, which are derived from the aircraft's planform curves' output by the geometry module.

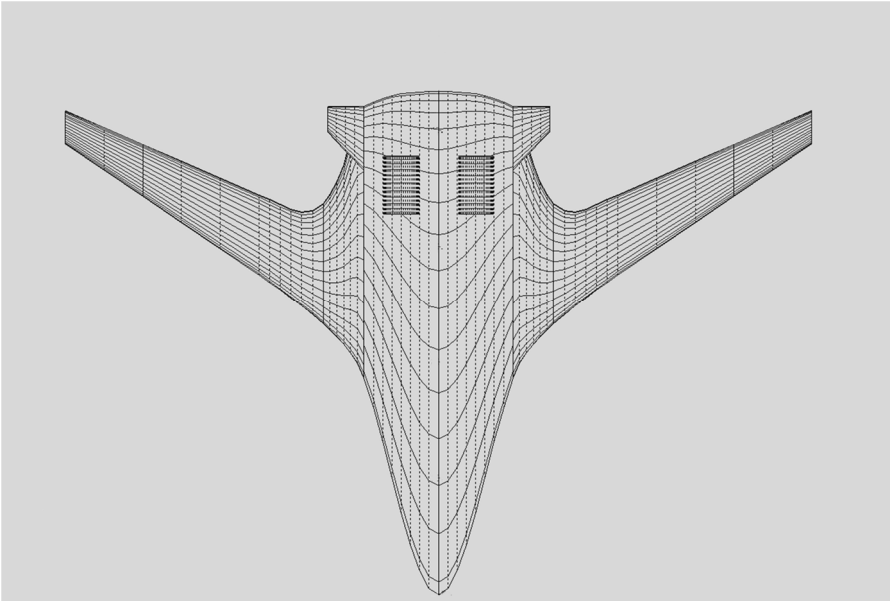


Figure 5. AVL mesh model of the HWB aircraft.

The second part is the airfoil, which corresponds to the three fuselage segments of the HWB civil aircraft—the center body, the blending area, and the outer wing. Each segment of the fuselage selects the corresponding airfoil according to its own functional characteristics Figure 6 [24]. The center fuselage airfoil is selected based on the following considerations: The first consideration was to choose an airfoil with both a suitable lift coefficient and the ability to achieve longitudinal aerodynamic moment balancing. For this purpose, an airfoil with a reflected camber design was selected, which allows the aerodynamic loads to be unloaded at the trailing edge of the airfoil to achieve pitch moment balancing. The second is the demand for a reasonable span-wise distribution of lift on the aircraft. Since the chord length of the center fuselage is longer than the other two segments, if the lift coefficients of the three airfoils are similar, the lift contributed by the center fuselage per unit span length will be excessive, and such a lift distribution is not conducive to drag reduction. So, the lift coefficient of the center fuselage airfoil should not be too large if the configuration is to obtain a reasonable lift distribution along the span. The transition-part airfoil, which is close to a symmetric airfoil, is used to achieve the airfoil transition between the outer wing section and the center fuselage. For the outer wing, a supercritical airfoil with a positive camber trailing-edge is used to ensure the transonic performance of the aircraft. In addition, the relative thickness of each airfoil is set with reference to the airfoil thickness distribution

in the literature [25]; that is, the spanwise thickness to chord ratio in the center fuselage section is 8% on average and reaches a maximum at the point of 0.16 of the full aircraft span, while the spanwise thickness-to-chord ratio of the outer-wing airfoil section is maintained at 8%. In addition, to ensure a positive zero-lift moment and aircraft balance, the airfoil twist needs to show a certain spanwise distribution, as shown in the Figure 7 where the center fuselage airfoil has a positive twist and the outer-wing airfoil has a negative twist. The flight conditions of the aerodynamic module are shown in Table 1, including the flight Mach number and altitude.

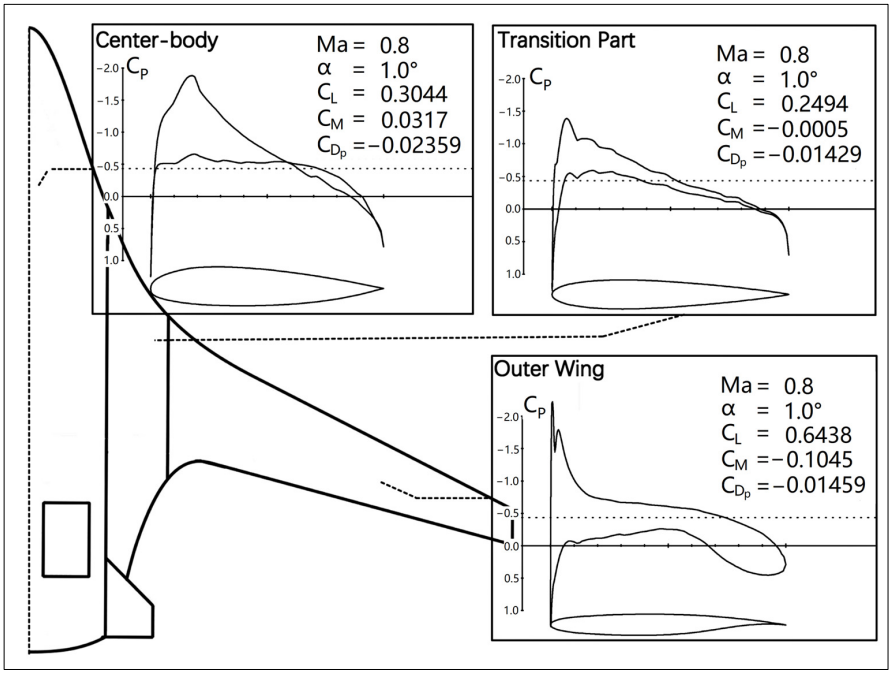


Figure 6. Airfoil sections of the HWB aircraft.

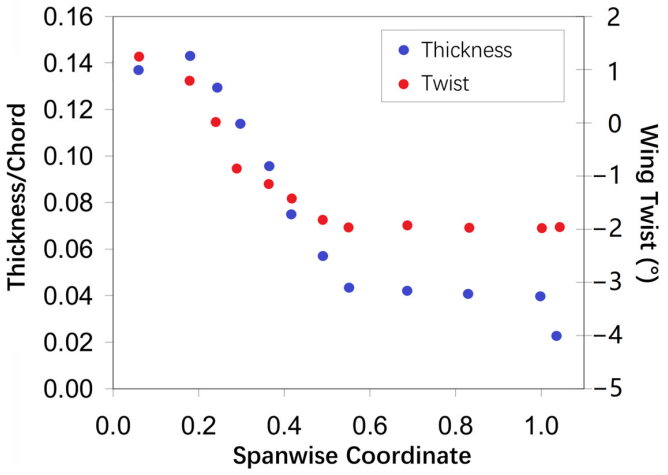


Figure 7. Spanwise distribution of the wing twist and airfoil thickness.

Table 1. Flight conditions.

Parameter	Value
Cruise Mach number	0.8
Cruise altitude, km	12

2.4. Trim Module

In the trim module, the first step is to trim the longitudinal forces of the design aircraft at cruising altitude and Mach number with zero deflection of the control surfaces to obtain the aircraft cruise attack angle. If the pitch moment of the aircraft is not zero at this attack angle, instead of using the control surface to trim the pitch moment, the longitudinal position of center of mass (derived from the weight module) is translated along the direction of the construction axis of the aircraft to achieve the trim of the longitudinal moment to maintain the neutral position of the control surface and thus to acquire a clean cruising configuration, and the translated distance is obtained by the Equation (7):

$$cg_{dis} = c_{ref}(C_m/C_{L0}). \tag{7}$$

In engineering practice, considering that the capability of aircraft to adjust position of center of mass is limited, the translation distance must be less than 7% of the average aerodynamic chord length in this procedure. Moreover, if cg_{dis} exceed this limit, it is determined that the design aircraft cannot satisfy the constraint of longitudinal aerodynamic moment trim at cruising state in the case of neutral position of control surface, and the optimization calculation should skip this cycle.

2.5. Stability and Control Characteristics' Calculation Module

In the stability and control characteristics' calculation module, firstly a group of pitch moment and lift coefficients are calculated at $\pm 0.4^\circ$, $\pm 0.8^\circ$, and $\pm 1.2^\circ$ of the cruise attack angle which is derived from the trim module. Based on the above group of data, we can fit the curve of lift coefficient and pitch moment coefficient with the angle of attack, the slope of the fitted curve is $C_{m\alpha}$ and $C_{L\alpha}$. Subsequently, $\frac{\partial C_m}{\partial C_L}$ is obtained according to Equation (8), and the static stability margin is obtained after changing the sign of $\frac{\partial C_m}{\partial C_L}$:

$$\frac{\partial C_m}{\partial C_L} = \frac{\partial C_m}{\partial C_\alpha} \Big/ \frac{\partial C_m}{\partial C_\alpha}, \tag{8}$$

Based on the equilibrium state points derived in the trim module, the linearized equations of small perturbations in the form of state space are obtained, and the corresponding short-period frequency, ω_{nsp}, and the control anticipant parameter, $\frac{\Delta n}{\Delta \alpha}$, are calculated. These two parameters are later used in the judging session as evidence for determining whether the aircraft has basic control authority, as mentioned above.

2.6. Validation of the Modules of MDO Platform

The SAX40 is selected to verify the three main calculation modules of MDO constructed in this paper for the following reasons: first, SAX40 is like the HWB aircraft studied in this paper in terms of seat stage and cross section airfoil; secondly, SAX-40 has more detailed mass and aerodynamic data to provide reference. The selected verification data include MTOW, cruise lift coefficient, drag coefficient, trim angle of attack, and so on. As can be seen from Table 2, the error between the calculated value and the reference data is within an acceptable range.

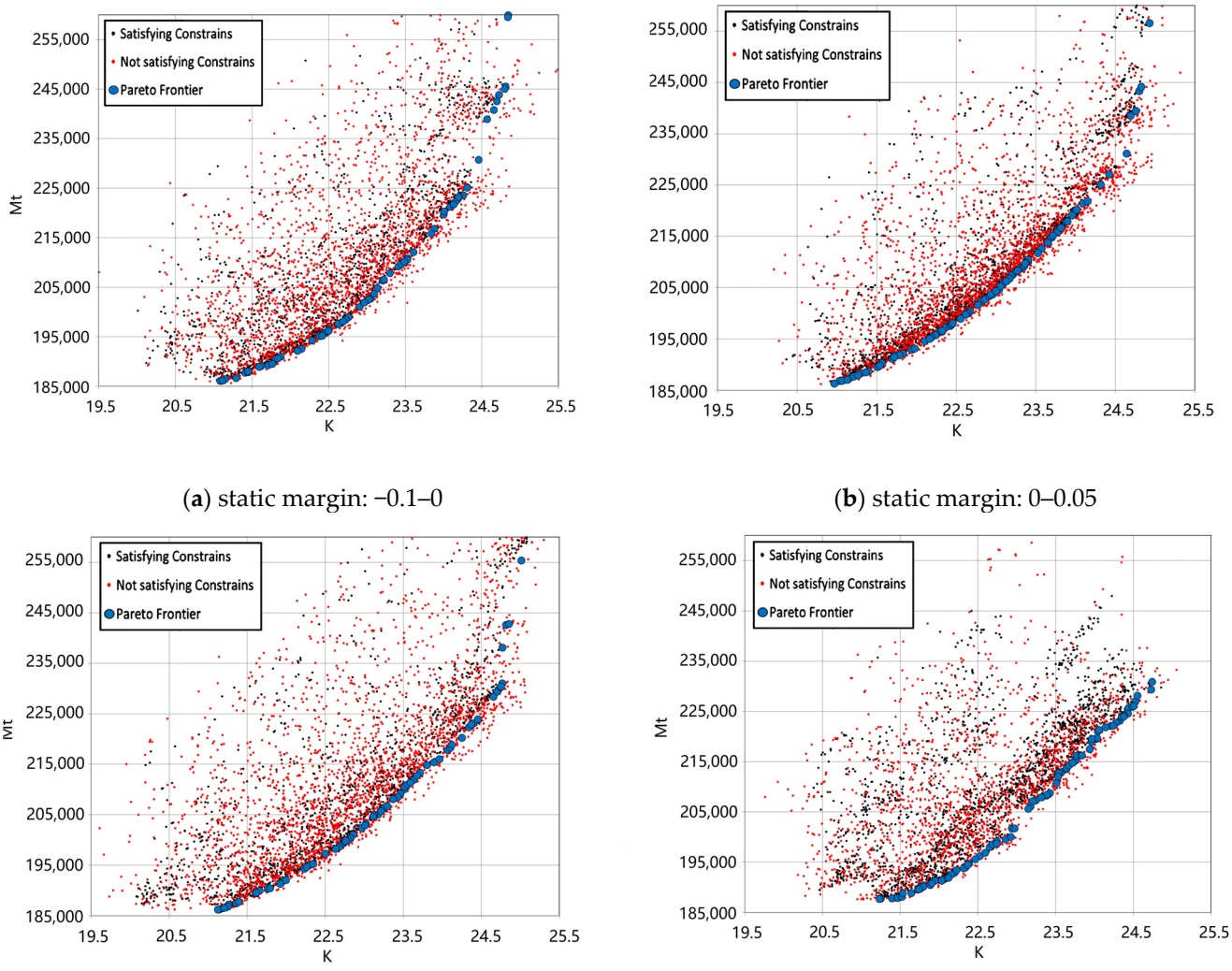
Table 2. Weight, aerodynamics, and trim validation with SAX-40 [21].

	Parameter	Ref.	Calculation	Δ(%)
Weight Module	MTOW, kg	150,846	155,510	3.1
Aerodynamic Module	C_L	0.2064	0.2083	0.9
	C_D	0.0082	0.0092	12.2
Trim Module	AOA, degree	2.7	2.99	10.7

3. Optimization Results

As mentioned in Section 2, this paper intends to set different static stability margin constraints in the optimization calculation to obtain different degrees of aft-body extension

design of HWB planform based on the significant influence of static stability margin on the planform of HWB aircraft. Specifically, the static stability margins in the range of −0.1–0.2 are divided into four intervals, namely −0.1–0, 0–0.05, 0.05–0.1, and 0.1–0.2, and then these four intervals are applied as constraints to four optimization tasks. The results of the optimization calculation are shown in Figure 8. Moreover, Figure 8 includes the scatter plots of the four sets of optimization results; each set of results corresponds to a specific static stability margin constraint range, where the blue points form the pareto frontier of each set of optimization calculations, the red points indicate that the sample point does not satisfy the optimization constraints, and the black points indicate that the sample point satisfies all the optimization constraints.



(**a**) static margin: −0.1–0

(**b**) static margin: 0–0.05

(**c**) static margin: 0.05–0.1

(**d**) static margin: 0.1–0.2

Figure 8. The optimization results under different static margin constraint.

The pareto frontiers of the four sets of optimization results are extracted and placed in the same coordinate system, and the points corresponding to these four pareto frontiers at k = 23.5 (the red line shown in Figure 9 are chosen to form the configuration family, which is used as the basis for the subsequent analysis. The four configurations of configuration family were named OPT1~4 according to the ascending order of static margin, and the planform of the configuration family is shown in Figure 10. We selected configurations according to a fixed lift–drag ratio, rather than the aft-body length, based on the following consideration: A single value of aft-body length on the pareto frontier may correspond

to multiple combinations of lift–drag ratio and weight and one combination may pareto dominate the other one, which made it difficult to choose a proper configuration from these combinations. So, we must determine the value of lift–drag ratio or weight before the choice of configuration for analysis. Considering that the lift–drag ratio is a more general parameter than weight, the data from other HWB designs can be used as a reference. At present, the cruise lift–drag ratio of HWB is generally between 22 and 24. [26,27] Combined with the calculation results in this paper, the design lift–drag ratio is determined to be 23.5.

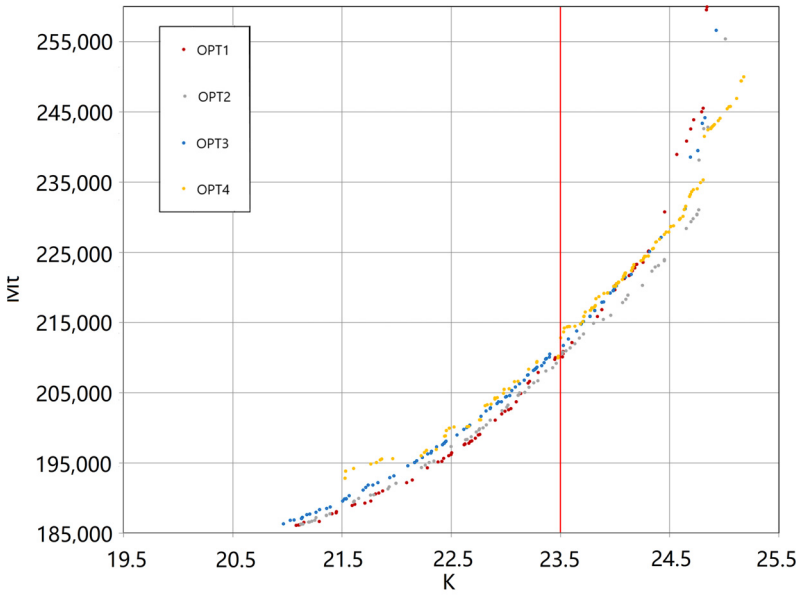


Figure 9. The pareto frontiers of the four optimization results.

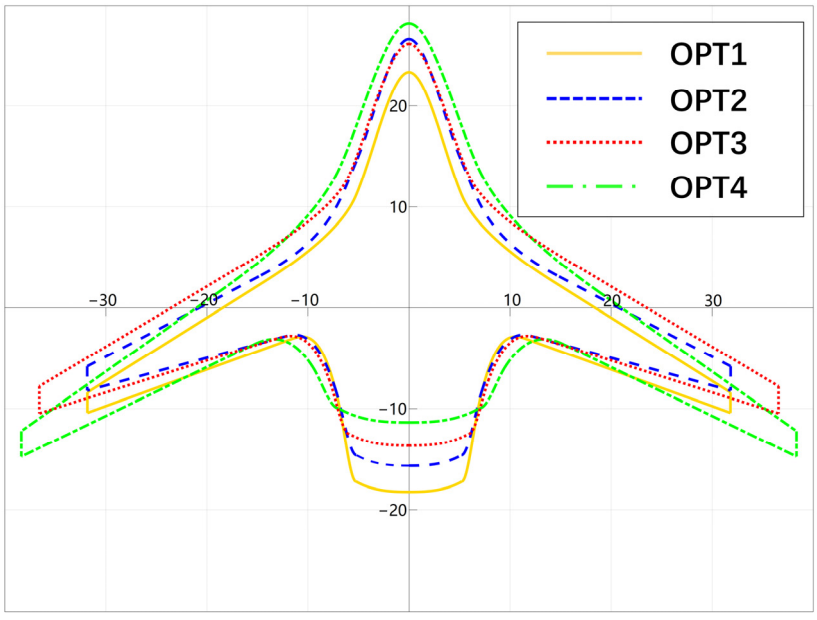


Figure 10. Planform of the configuration family.

Figure 10 shows that, for the HWB configuration, the smaller the longitudinal static stability margin, the more forward the outer wing moves, and the longer the aft-body length is. The fundamental reason for this phenomenon is that the aft-body extension design causes a larger shift of the center of mass backward compared to the aerodynamic center. This difference in offset distance results in lower static stability margins for con-

figurations with aft-body extensions and higher static stability margins for short fuselage configurations.

4. Characteristics Evaluation

This section focuses on the weight, basic takeoff and landing performance, and control authority of the four configurations within the configuration family mentioned above to derive the effect of aft-body extension design on the main characteristics of the HWB aircraft.

4.1. Weight Analysis

The MTOWs of the four configurations are shown in Table 3, and the MTOWs of the OPT4 to OPT1 aircraft are gradually decreasing. Since the masses of the non-structural parts are set to constant values in this paper, it can be concluded that, with the extension of aft-body, a slight reduction in the total structural mass of the aircraft can be achieved.

Table 3. MTOWs of four HWB configurations.

Aircraft Configuration	OPT1	OPT2	OPT3	OPT4
MTOW, kg	209,664	210,798	211,495	213,406

4.2. Basic Takeoff and Landing Performance Analysis

4.2.1. Takeoff Performance Analysis

The basic takeoff performance of these four aircraft configurations was evaluated based on two parameters: the rotary speed and the takeoff field length. The calculation of rotary speed and takeoff glide distance for HWB aircraft is based on the following three conditions: First, the HWB aircraft accelerates to the rotary speed in the ground state, and at this speed, the aircraft can generate the specified angular acceleration by deflecting the elevons within a limited angular range. Second, after the rotation, the pitch moment of the aircraft is balanced with a slight restoration of control surface, so that the aircraft can be stabilized in a suitable takeoff attitude. Third, based on the takeoff attitude calculated by the second condition and takeoff speed (takeoff speed is about 1.1 times of rotary speed), the lift generated by the aircraft can offset the gravity to achieve the off-ground action.

When calculating the rotary speed and takeoff glide distance, care should be taken to keep the deflection angle of the elevons within a reasonable range to avoid excessive deflection. This is mainly due to two considerations. On the one hand, it is a common problem for every aircraft when lifting the nose; that is, too much deflection will increase the restoration of control surface after leaving the ground, which will cause drastic changes in attitude of aircraft and deteriorate the controller quality. Another aspect is the unique problem of HWB aircraft. Since the lift surface and control surface of the HWB are highly integrated, a large control surface deflection will lead to a serious loss of lift, which will make the takeoff attack angle too large and affect the normal takeoff of the aircraft. From the comprehensive view of the literature, the upper limit of elevon deflection angle is set here to $\pm 15^\circ$ when rotating the HWB aircraft.

The elevon deflection angle is deflected to the upper limit, and then the rotary speed is derived by the Equation (9), which requires that the pitch aerodynamic moment generated by the elevon deflection at this speed be sufficient to lift the nose of the aircraft and produce the specified instantaneous angular acceleration:

$$I_y\ddot{\theta} = qS\left[cC_m(\alpha,\delta_e) + C_L(\alpha,\delta_e)\left(x + fy_g\right)\right] - (G - Tsin\alpha)\left(x + fy_g\right) - Ty_p \quad (9)$$

where $\ddot{\theta}$ is the angular acceleration generated by the pitch moment of the whole aircraft at the instant of rotation; $\ddot{\theta}$ is set to $3^\circ/s^2$ according to the general rule of rotation for blended wing-body aircraft [28]. Moreover, x is the horizontal distance from the aircraft's center of gravity to the wheel axis of main landing gear. This value can be calculated by the weight ratio carried by the main landing gear and front landing gear (in this paper this

ratio is set to 9:1) and the position of the center of gravity. Furthermore, f is the rolling friction coefficient of the wheel of the main landing gear and y_g is the plumb distance from the center of gravity to the ground. Based on the already derived rotary speed, a rough estimate of the gliding distance required for the entire takeoff process can be obtained.

The takeoff performance calculation results for the four configurations within the configuration family are shown in Figure 11, in addition to the takeoff data for the B777 in the same class of civil aircraft for comparison. The blue bars in the figure indicate the rotary speed, and the gray bars indicate the gliding distance. First, it can be concluded from the figure that the aft-body extension design can improve the takeoff performance of HWB aircraft, but there is still a gap between the takeoff performance of HWB civil aircraft and conventional TAW aircraft, and even the OPT1 aircraft with the largest degree of aft-body extension design cannot achieve the takeoff and gliding performance of the same class of TAW. Secondly, although the overall trend shows that the takeoff performance can be improved with the aft-body extension, the comparison of the takeoff data of aircraft OPT2 and OPT3 show that the effect of the aft-body extension design on the improvement of the takeoff performance is disturbed because the takeoff performance depends not only on the control arm of the aircraft but also on the ground-support reaction moment, which is mainly affected by the spacing between the center of mass and the main landing gear of the aircraft. In other words, the takeoff performance depends not only on the relative position of the center of mass to the aerodynamic center but also on the absolute position of the center of mass.

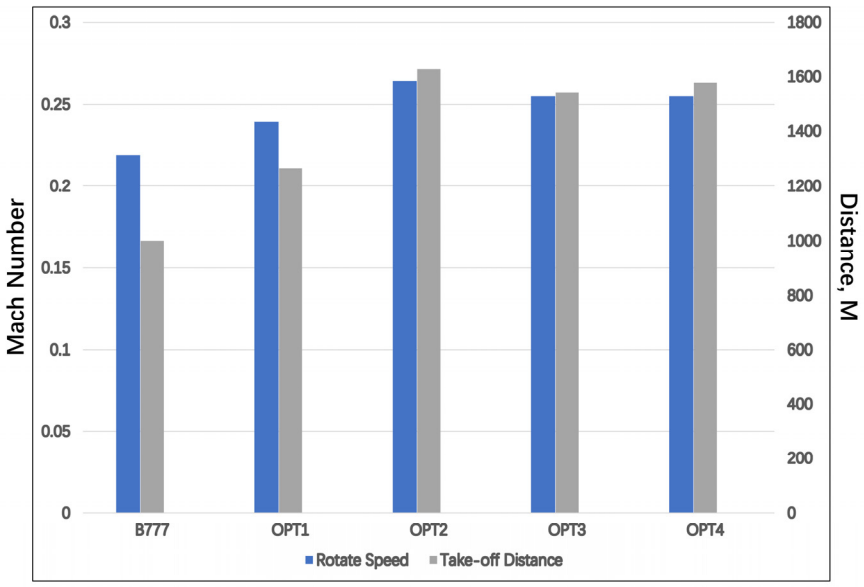


Figure 11. Takeoff performance for the four configurations.

4.2.2. Landing-Performance Analysis

This subsection is an evaluation of the basic landing performance of these four configurations of aircraft. As mentioned in this paper, the HWB aircraft is a kind of configuration with high integration of the lift surface and control surface, and the upward deflection of the elevons during landing will destroy the lift surface's aerodynamic shape and cause significant lift loss at the trailing edge of the aircraft, so the angle of attack in the landing process needs to be increased to supplement the lift. Due to the large landing angle of attack, the lateral stability of the HWB layout aircraft in landing is poor, and there is even a risk of Spiral mode dispersion, which is not conducive to landing safety [29]. In summary, the evaluation of the basic landing performance of the four configurations focuses on the trim angle of attack in the landing process and the modal performance of the aircraft at low speed.

The final calculation results of the landing performance are shown in Figures 12 and 13, where Figure 12 reflects the landing angle of attack of each type of aircraft in the configuration family, and Figure 13 reflects the motion modes in the landing state. From Figure 12, we can see that the aft-body extension can significantly decrease the landing angle of attack of the aircraft, where the OPT1 aircraft can even reach the level of the same class of TAW aircraft, while the shortest aft-body, OPT4 aircraft, has the angle of nearly 15 degrees. From Figure 13, it is obvious that the Spiral mode of the aircraft is significantly improved with the aft-body extension, and the convergence of Spiral mode is finally achieved on OPT1 aircraft.

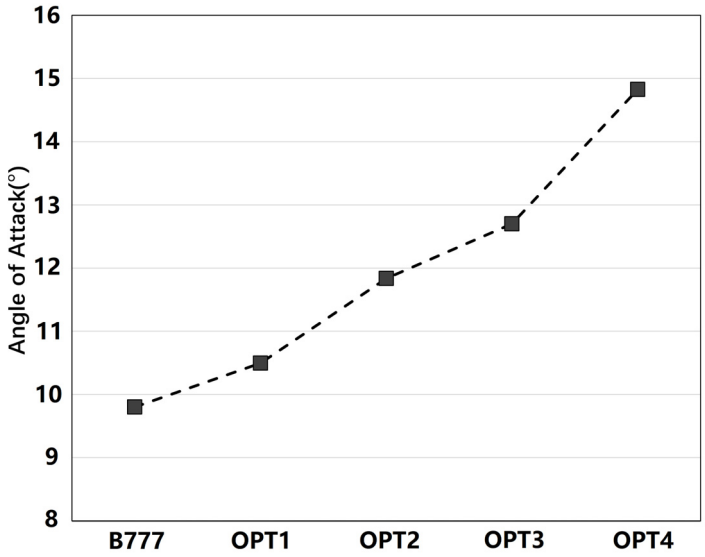


Figure 12. Landing angle of attack of each type of aircraft in the configuration family.

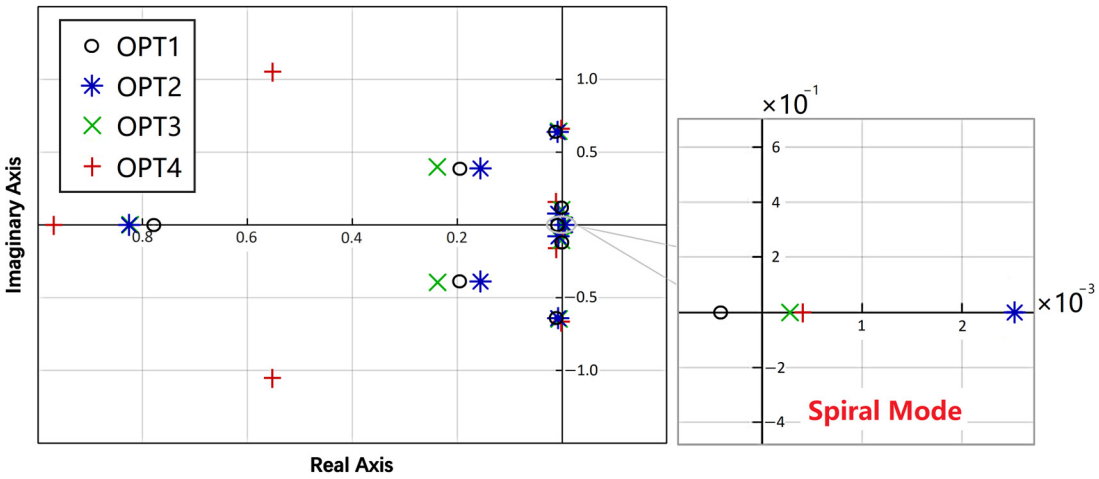


Figure 13. Poles of aircraft dynamics for landing status of four configurations.

4.3. Flight Control Authority Evaluation

The evaluation of the control authority of these four configurations of aircraft focuses on comparing their required additional deflection angles of control surface, i.e., $\frac{\partial \delta_e}{\partial n_n}$, for changing unit normal overload at the balance condition. In the calculation, the deflection of elevon required for the trim at the situation point is generally found first, and then the deflection of elevon required for maneuvering is calculated based on it. It should be noted that the focus of this paper is to compare the longitudinal control authority of these four configurations rather than to assess the maneuvering capability of specific configurations within the full envelope in detail and comprehensively; thus, for each configuration, only a

few speed points between Mach 0.4 and 0.8 are selected for the trim and calculation. The $\frac{\partial \delta_e}{\partial n_n}$ can be obtained by Equation (10):

$$\frac{\partial \delta_e}{\partial n_n} = -\frac{\left(\frac{\partial C_m}{\partial C_L} + \frac{C_{mq}}{\mu_1}\right)}{C_{m\delta_e}} \frac{W}{qS}, \tag{10}$$

where μ_1 is the relative density of the aircraft.

The calculated results for the control authority of the four configurations are shown in Figure 14. According to the results, we have the following conclusions. First, the aft-body extension improves the control authority of the HWB aircraft at both high and low speeds. The comparison of OPT3 and OPT4 and the comparison of OPT2 and OPT3 especially shows that the initial improvement effect of the aft-body extension to control authority is significant. On the other hand, from the comparison of Aircraft 1 and 2, this improvement effect decays when the aft-body is extended to a certain degree. Secondly, the difference in control authority of each configuration at high speed is not as large as that at low speed, so the aft-body extension shows much importance in improving the control authority of HWB aircraft at low-speed operation.

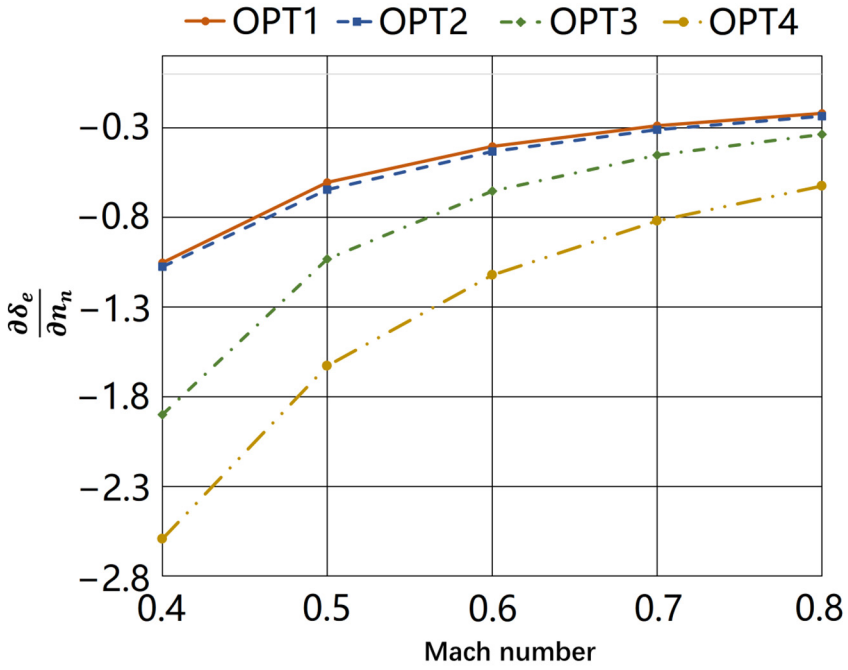


Figure 14. The control authority of the four configurations at different Mach number.

5. Conclusions

To study the influence of the HWB aft-body extension design on the performances of aircraft, this article calculated the MTOW, basic takeoff and landing performance, and control authority of four HWB configurations. The following conclusions can be obtained after a comparison and analysis of the calculation results:

1. The correlation between the degree of aft-body extension and MTOW of aircraft is changed over the whole range of lift-to-drag ratio. When it comes to the range around the design's lift-to-drag ratio, there is a slight reduction in MTOW with the increase in extension of aft-body fuselage. Therefore, without considering the influence of secondary power consumption, etc., aft-body extension has a positive impact on the operation economy of the aircraft.
2. In terms of general trend, aft-body extension design can moderately improve the takeoff performance of HWB aircraft, but aft-body extension design alone cannot enable HWB aircraft to reach the level of the takeoff performance of the same seat-class

TAW civil aircraft. Obviously, additional measures are needed to improve the takeoff performance of HWB aircraft, such as vectoring thrust systems.

3. The landing angle of attack can be significantly reduced through aft-body extension design. Moreover, the HWB's Spiral mode during landing has been significantly improved due to the decrease in the landing angle of attack, which is reflected in the fact that the configuration with the aft-body extension achieves convergence of the Spiral mode compared to the divergence of Spiral mode of the short fuselage configuration.
4. The aft-body extension design has improved the flight control authority of the HWB aircraft at both high and low speeds, and this improvement effect is more obvious at low speed. The marginal effect should also be noted: the improvement on the flight control authority will be significantly reduced when the aft-body is extended to a certain length.

Author Contributions: Y.W. performed the main work of this article, including the conception of this study, calculations, and manuscript writing; G.L. and G.H. contributed significantly to the analysis of computations and the revision of this article. All authors have read and agreed to the published version of the manuscript.

Funding: This research received no external funding.

Conflicts of Interest: The authors declare no conflict of interest.

Nomenclature

HWB	Hybrid Wing Body
BWB	Blended Wing Body
TAW	Tube and Wing
MTOW	Maximum Takeoff Weight
MDO	Multidiscipline Design Optimization
AOA	angle of attack
NSGA	Nondominated Sorting Genetic Algorithm
CFD	Computational Fluid Dynamics
r	wing bending relief factor
c	chord of the wing section (m)
τ	maximum airfoil thickness—chord ratio
S	wing planform area (m^2)
S'	idealized wing planform area (m^2)
$\overline{f_a}$	ratio of the allowable compressive stress to the upper limiting value
C_m	moment coefficient in pitch axis
C_L	lift coefficient
C_{L0}	lift coefficient on cruise speed
$C_{L\alpha}$	$\partial C_L / \partial \alpha$
θ	pitch angle (rad)
δ_e	deflection angle of elevator (rad)
$C_{m\delta_e}$	$\partial C_m / \partial \delta_e$
C_{mq}	$\partial C_m / \partial q$
μ_1	relative density of the aircraft
q	dynamic pressure (Pa)
α	attack angle (rad)

References

1. Liebeck, R.H. Design of the Blended Wing Body Subsonic Transport. *J. Aircr.* **2004**, *41*, 10–25. [CrossRef]
2. Potsdam, M.A.; Page, A.M.; Liebeck, R.H. Blended wing body analysis and design. In Proceedings of the 15th Applied Aerodynamics Conference, Reston, VA, USA, 23–25 June 1997.
3. Ordoukhanian, E.; Madni, M.A. Blended wing body architecting and design: Current status and future prospects. *Procedia Comput. Sci.* **2014**, *28*, 619–625. [CrossRef]

4. Chen, Z.L.; Zhang, M.H. Assessment on critical technologies for conceptual design of blended-wing-body civil aircraft. *Chin. J. Aeronaut.* **2019**, *32*, 1797–1827. [CrossRef]
5. Reist, T.A.; Zingg, D.W. Aerodynamic design of blended wing-body and lifting-fuselage aircraft. In Proceedings of the 34th AIAA Applied Aerodynamics Conference, Washington, DC, USA, 13–17 June 2016.
6. Okonkwo, P.; Smith, H. Review of evolving trends in blended wing body aircraft design. *Prog. Aerosp. Sci.* **2016**, *82*, 1–23. [CrossRef]
7. Reist, T.A.; Zingg, D.W. Optimization of the aerodynamic performance of regional and wide-body-class blended wing-body aircraft. In Proceedings of the 33rd AIAA Applied Aerodynamics Conference, Dallas, TX, USA, 22–26 June 2015.
8. Nickol, C. Hybrid wing body configuration scaling study. In Proceedings of the 50th AIAA Meeting, Nashville, TN, USA, 9 January 2012.
9. Rauno, C.; Rocco, B. Studies on Lateral-directional Coupled Flight Dynamics and Aeroelasticity of a PrandtlPlane. In Proceedings of the AIAA Scitech 2019 Forum, San Diego, CA, USA, 7–11 January 2019.
10. Luciano, D.; Rauno, C.; Alan, M.R. Postcritical Analysis of PrandtlPlane Joined-Wing Configurations. *AIAA J.* **2012**, *51*, 1700.
11. Hall, C.A.; Schwartz, E.; Hileman, J.I. Assessment of technologies for the Silent Aircraft Initiative Title. *J. Propul. Power* **2009**, *25*, 1153. [CrossRef]
12. Almosnino, D. A low subsonic study of the NASA N2A hybrid wing-body using an inviscid Euler. In Proceedings of the 34th AIAA Applied Aerodynamics Conference, Washington, DC, USA, 13–17 June 2016.
13. Kim, H.; Liou, M.S. Shape design optimization of embedded engine inlets for N2B hybrid wing-body configuration. *Aerosp. Sci. Technol.* **2013**, *30*, 128–149. [CrossRef]
14. Feldstein, A.W.; Lazzara, D.; Princen, N.; Willcox, K.E. Model uncertainty: A challenge in nonlinear coupled multidisciplinary system design. In Proceedings of the 2018AIAA/ASCE/AHS/ASC Structure, Structural Dynamics, and Materials Conference, Kissimmee, FL, USA, 8–12 January 2018.
15. Wang, G.; Zhan, M.H.; Tao, Y.J. Research on analytical scaling method and scale effects for subscale flight test of blended wing body civil aircraft. *Aerosp. Sci. Technol.* **2020**, *106*, 106–144. [CrossRef]
16. Hooker, J.R.; Wick, A. Design of the hybrid wing body for fuel efficient air mobility operations. In Proceedings of the 52nd Aerospace Sciences Meeting, National Harbor, MA, USA, 13–17 January 2014.
17. Roman, D.; Allen, J.; Liebeck, R.H. Aerodynamic design challenges of the blended-wing-body subsonic transport. In Proceedings of the 18th AIAA Applied Aerodynamics Conference, Denver, CO, USA, 14–17 August 2000.
18. Lyu, Z.; Martins, J.R.R.A. Aerodynamic design optimization studies of a blended wing body aircraft. *J. Aircr.* **2014**, *51*, 5. [CrossRef]
19. Reist, T.A.; Zingg, D.W. Multi-fidelity Optimization of Hybrid wing-body aircraft with stability and control requirements. *J. Aircr.* **2018**, *56*, 2.
20. Zhang, M.H.; Chen, Z.L. Effects of stability margin and thrust specific fuel consumption constrains on multi-disciplinary optimization for blended-wing-body design. *Chin. J. Aeronaut.* **2019**, *32*, 1847–1859. [CrossRef]
21. Hileman, J.; Spakovszky, Z.; Drela, M.; Sargeant, M. Airframe design for "silent aircraft". In Proceedings of the 45th AIAA Aerospace Sciences Meeting and Exhibit, Nashville, TN, USA, 9 January 2012.
22. Bradley, K. *A Sizing Methodology for the Conceptual Design of Blended-Wing-Body Transport*; George Washington University, Joint Institute for the Advancement of Flight Sciences, Langley Research Center: Hampton, VA, USA, 2004.
23. Howe, D. Blended wing body airframe mass prediction. *J. Aerosp. Eng.* **2001**, *215*, 6. [CrossRef]
24. Rahman, N.U.; Whidborne, J.F. Propulsion and flight controls integration for a blended-wing-body transport aircraft. *J. Aircr.* **2010**, *47*, 6. [CrossRef]
25. Qin, N.; Vavalle, A. Aerodynamic considerations of blended wing body aircraft. *Prog. Aerosp. Sci.* **2004**, *40*, 321–343. [CrossRef]
26. Aiden, G.; Thomas, R.; David, W.Z. Further Exploration of Regional-Class Hybrid Wing-Body Aircraft Through Multifidelity Optimization. In Proceedings of the AIAA Scitech 2021 Forum, Online, 11–21 January 2021.
27. Yu, C.; Jiacheng, X.; Evan, H.; Dimitri, M. Assessment of Longitudinal Stability-and-Control Characteristics of Hybrid Wing Body Aircraft in Conceptual Design. In Proceedings of the AIAA Aviation 2021 Forum, Online, 2–6 August 2021.
28. Bonet, J.T.; Schellenger, H.G.; Rawdon, B.K.; Wakayama, D.L.; Brown, D.L. *Environmentally Responsible Aviation (ERA) Project-N+2 Advanced Vehicle Concepts Study and Conceptual Design of Subscale Test Vehicle (STV)-Final Report*; Report No.: NASA/CR-2011-216519; NASA Dryden Flight Research Center: Washington, DC, USA, 2011.
29. Wildschek, A. Flight dynamics and control related challenges for design of a commercial blended wing body aircraft. In Proceedings of the AIAA Guidance, Navigation, and Control Conference, National Harbor, MA, USA, 13–17 January 2014.